


Particle creation and annihilation in a dynamically disordered totally asymmetric simple exclusion process

Shaweta Garg and Isha Dhiman*

School of Mathematics, Thapar Institute of Engineering and Technology, Patiala 147001, Punjab, India

 (Received 22 November 2020; revised 1 March 2021; accepted 3 May 2021; published 17 May 2021)

We study a single-channel dynamically disordered totally asymmetric simple exclusion process with bulk particle attachment and detachment. The continuum mean-field equations are derived and solved numerically to obtain steady-state phase diagrams and density profiles. The effects of various parameters, namely particle attachment rate, defect binding and unbinding rates, and binding constant, have been investigated. An increase in the attachment rate of particles reduces the number of steady-state phases, whereas a variation in defect binding and unbinding rates shifts the phase boundaries. One of the important consequences of introducing particle nonconserving dynamics is the appearance of shock in the steady state. The shock dynamics have been thoroughly examined and the defect strength is found to have a significant effect on the shock position. The mean-field solutions are validated using extensive Monte Carlo simulations.

DOI: [10.1103/PhysRevE.103.052120](https://doi.org/10.1103/PhysRevE.103.052120)

I. INTRODUCTION

Intracellular transport of cargoes in eukaryotic cells is accelerated by motor proteins which move along filamentary tracks called microtubules. The motor proteins are enzymatic molecules that convert chemical energy, derived from hydrolysis of adenosine triphosphate (ATP), into mechanical energy [1,2]. The motor proteins often encounter roadblocks which slow down the transportation process [3]. Specifically, transcription of genetic information stored in DNA is carried out by a molecular motor called RNA polymerase (RNAP). The RNAP synthesizes an RNA transcript to create messenger RNA (mRNA) which is composed of a sequence of codons [4–7]. The mRNA is decoded in ribosomes to form amino acid chains. During translation, individual amino acids are transferred by the transfer RNA (tRNA) and are then chained together to form a polypeptide or protein. The DNA binding proteins during transcription and the low concentration of tRNA during translation act as bottlenecks in the system. The presence of bottlenecks may cause jams on the microtubule track. The slow transport of cargoes within the cell due to jamming may result in neurodegenerative diseases like Alzheimer’s and amyotrophic lateral sclerosis (ALS) [8].

Intracellular transport is characterized as a far-from-equilibrium system due to continuous supply of energy that maintains nonzero flux in the system. The simplest statistical physics model, the totally asymmetric simple exclusion process (TASEP) [7,9,10] well describes the transport phenomena of such nonequilibrium systems. It is a stochastic model accounting movement of particles along a track. These tracks are one-dimensional lattices on which particles proceed in a preferred direction obeying a hard-core exclusion principle with certain preassigned rules. The nature of the

nonequilibrium steady-state of TASEP depends sensitively on the boundary conditions. The most interesting phenomena revealed by open boundary conditions are phase separations and boundary induced phase transitions [11–13].

Despite its simplicity, TASEP and its extensions have also been used to describe a number of complex natural phenomena. Due to finite processivity, motor proteins diffusing freely can attach to the microtubule filament and can also detach from the microtubule to the cytoplasm. The process of attachment and detachment has been named Langmuir kinetics (LK) in the literature [14,15]. The inclusion of LK dynamics violates the particle conservation in the bulk and exhibits additional feature, namely localization of shock. The coupling of TASEP with LK has been extensively studied in single-channel [16–18] as well in two-channel homogeneous systems [19–22].

The slowing down of motor proteins due to the presence of a bottleneck while processing over the microtubule track leads to inhomogeneity in the system. The case of static inhomogeneity, where the position of defect is fixed at a particular site on the lattice, has been extensively studied in TASEPs with as well as without LK [23–35]. Importantly, the above mentioned studies focused mainly on static inhomogeneity.

In the process of gene transcription motor proteins are also encountered by defects that are dynamic, i.e., the defects appear and disappear dynamically [36,37]. In particular, RNAP comes across bottlenecks caused by DNA binding proteins such as histones which interrupt RNA chain elongation dynamically [38]. This sheds light on the importance of considering dynamic disorder in nonequilibrium systems. From our viewpoint, the case of dynamic disorder has been less studied in comparison to static disorder. Recently, single-channel TASEP with dynamic disorder (ddTASEP) was investigated by Waclaw *et al.* [38]. Garg and Dhiman [39] explored the role of dynamic disorder in two-channel TASEP without LK in a symmetric coupling environment.

*isha@thapar.edu

Dynamically disordered TASEP with LK has not yet been studied to the best of our knowledge. The aim of this paper is to explore the role played by dynamic disorder in TASEP (ddTASEP) with LK.

The paper is organized as follows. The model and dynamical rules are defined in Sec. II. The continuum mean-field equations are derived in Sec. III. The numerical techniques to solve continuum mean-field equations and Monte Carlo simulations are explained in Sec. IV. The phase diagrams, density profiles, and effects of various parameters are discussed in detail in Secs. V and VI. Lastly, in Sec. VII, we summarize the outcomes and mention possible future studies.

II. MODEL DESCRIPTION

The proposed model consists of a one-dimensional open lattice channel with dynamic disorder and Langmuir kinetics having L sites (ddTASEP with LK). The particles are distributed under the hard-core exclusion principle, which means that each lattice site can be either vacant or occupied by exactly one particle. The state of the system is defined by two sets of occupation numbers: one for particles denoted by τ_i and another for defects denoted by v_i at i th site of the lattice, where $i = 1, 2, 3, \dots, L$. Each of τ_i and v_i can take value either 0 or 1, 0 representing absence of particle or defect and 1 representing presence of particle or defect. For each time step, a lattice site i ($i = 1, 2, 3, \dots, L$) is randomly chosen according to random-sequential update rules. At any site on the lattice, a defect can bind or unbind with rate k_+ or k_- respectively. The defect dynamics are unconstrained in which defect binding to a site is independent of presence of particle at that site [38]. The evolution of the system from one state to another occurs according to the following dynamical rules.

(i) At the entrance, i.e., $i = 1$, a particle can enter the lattice with a rate α provided $\tau_i = 0$ and $v_i = 0$. In other words, for a particle to enter the lattice, the first site should be particle free as well as defect free.

(ii) At the exit, i.e., $i = L$, a particle can leave the lattice with a rate β if $\tau_i = 1$ irrespective of $v_i = 0$ or 1.

(iii) In the bulk, i.e., $i = 2, 3, \dots, L - 1$, if $\tau_i = 1$, then the particle at the i th site first tries to detach itself from the lattice with detachment rate ω_d , and if it fails to detach then it hops forward to the $(i + 1)$ th site with a rate p_i provided $\tau_{i+1} = 0$, where

$$p_i = \begin{cases} p & \text{if } v_{i+1} = 0, \\ p_d & \text{if } v_{i+1} = 1. \end{cases}$$

On the other hand, if $\tau_i = 0$, a particle can attach to the lattice with attachment rate either ω_a if $v_{i+1} = 0$, i.e., the target site is defect free, or ω_{ad} if $v_{i+1} = 1$, i.e., the target site has a defect.

The hopping rate p_d , $0 \leq p_d \leq p$, is the slow forward hopping rate in the presence of a defect at the target site. A schematic representation of totally asymmetric exclusion process with dynamic disorder and Langmuir kinetics is shown in Fig. 1.

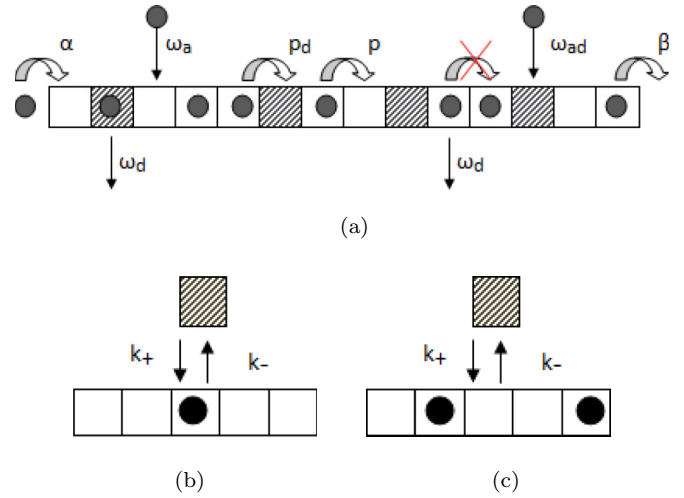


FIG. 1. (a) Schematic diagram of a single-channel TASEP with dynamic disorder and Langmuir kinetics. The dynamic defect is represented as a shaded site. Crossed arrows indicate forbidden transitions. Illustration of unconstrained defect dynamic (b) in the presence and (c) in the absence of a particle at the target site.

III. MASTER EQUATIONS

A. Particle density evolution

The temporal evolution of the average site occupation number $\langle \tau_i \rangle$ for any site in the bulk i ($2 \leq i \leq L - 1$) is obtained from the following set of master equations:

$$\begin{aligned} \frac{d\langle \tau_i \rangle}{dt} = & p\langle \tau_{i-1}(1 - \tau_i)(1 - v_i) \rangle + p_d\langle \tau_{i-1}(1 - \tau_i)(v_i) \rangle \\ & - p\langle \tau_i(1 - \tau_{i+1})(1 - v_{i+1}) \rangle - p_d\langle \tau_i(1 - \tau_{i+1})(v_{i+1}) \rangle \\ & + \omega_a\langle (1 - \tau_i)(1 - v_i) \rangle + \omega_{ad}\langle (1 - \tau_i)(v_i) \rangle \\ & - \omega_d\langle \tau_i \rangle, \end{aligned} \quad (1)$$

where $\langle \dots \rangle$ denotes the statistical average. Here, the first four terms on the right-hand side represent particle forward hopping obeying the hard-core exclusion principle and the last three terms describe the gain and loss arising due to particle attachment and detachment. At the boundaries, the particle density evolves as

$$\begin{aligned} \frac{d\langle \tau_1 \rangle}{dt} = & \alpha\langle (1 - \tau_1)(1 - v_1) \rangle - p\langle \tau_1(1 - \tau_2)(1 - v_2) \rangle \\ & - p_d\langle \tau_1(1 - \tau_2)(v_2) \rangle, \end{aligned} \quad (2)$$

$$\begin{aligned} \frac{d\langle \tau_L \rangle}{dt} = & p\langle \tau_{L-1}(1 - \tau_L)(1 - v_L) \rangle + p_d\langle \tau_{L-1}(1 - \tau_L)(v_L) \rangle \\ & - \beta\langle \tau_L \rangle. \end{aligned} \quad (3)$$

B. Defect density evolution

The defect density for lattice site i ($i = 1, 2, 3, \dots, L$) is given by

$$\frac{d\langle v_i \rangle}{dt} = k_+\langle 1 - v_i \rangle - k_-\langle v_i \rangle. \quad (4)$$

C. Continuum mean-field equations

Factorizing the correlations as product of their averages using mean-field approximation, we get

$$\langle \tau_i \tau_{i+1} \rangle = \langle \tau_i \rangle \langle \tau_{i+1} \rangle. \quad (5)$$

To obtain the continuum description of the model in the hydrodynamic limit $L \rightarrow \infty$, we coarse grain the discrete lattice with lattice constant $\epsilon = 1/L$ ($x \in [0, 1]$), and rescale the time as $t' = t/L$. The system reaches steady state only due to particle conserving dynamics as the nonconserving dynamics occurs at slower rate in contrast to the conserving dynamics. To ensure the competing interplay between the particle conserving and nonconserving dynamics, we rescale the attachment and detachment rates in such a way that the kinetic rates decrease simultaneously with an increase in the system size. Such rescaling is well employed in the literature [15,31,39]. Therefore, we have $\Omega_a = \omega_a L$, $\Omega_{ad} = \omega_{ad} L$, and $\Omega_d = \omega_d L$.

Replacing the binary discrete variable τ_i with a continuous variable $\rho_i \in [0, 1]$ and performing Taylor's series expansion up to second order, we get

$$\rho_{i\pm 1} = \rho_i \pm \frac{1}{L} \frac{\partial \rho_i}{\partial x} + \frac{1}{2L^2} \frac{\partial^2 \rho_i}{\partial x^2} + O\left(\frac{1}{L^3}\right). \quad (6)$$

The system transitions are site independent as each site in the bulk has equivalent dynamical rules, so we can drop the subscript i . The continuum mean-field equation in terms of the average density $\rho(x, t')$ governing the state of the system is depicted as

$$\begin{aligned} \frac{\partial \rho}{\partial t'} &= \frac{\epsilon}{2} (p - p\rho_d + p_d\rho_d) \frac{\partial^2 \rho}{\partial x^2} \\ &\quad - (p - p\rho_d + p_d\rho_d)(1 - 2\rho) \frac{\partial \rho}{\partial x} \\ &\quad + \Omega_a(1 - \rho)(1 - \rho_d) + \Omega_{ad}(1 - \rho)\rho_d - \Omega_d\rho. \end{aligned} \quad (7)$$

Similarly, Eqs. (2) and (3) in steady state are translated to

$$\rho(0) = \frac{\alpha(1 - \rho_d)}{\rho_d p_d + (1 - \rho_d)p}, \quad \rho(1) = 1 - \frac{\beta}{\rho_d p_d + (1 - \rho_d)p}. \quad (8)$$

with the particle current J given by

$$J = [\rho_d p_d + (1 - \rho_d)p] \rho(1 - \rho). \quad (9)$$

Equation (4) representing the average defect density gives

$$\rho_d = \frac{k_+}{k_+ + k_-}. \quad (10)$$

This expression for defect density is the same as that observed in Ref. [38].

IV. NUMERICAL SOLUTION AND MONTE CARLO SIMULATIONS

In this section, we describe the numerical scheme to solve the system of equations (7) and (8) and Monte Carlo simulations to compute the steady-state density profiles and the average current.

A. Steady-state equation

To compute the steady-state solution of the system, the left-hand side of Eq. (7) vanishes and we need to solve the following equation along with the boundary conditions represented by Eq. (8):

$$\begin{aligned} \frac{\epsilon}{2} (p - p\rho_d + p_d\rho_d) \frac{d^2 \rho}{dx^2} - (p - p\rho_d + p_d\rho_d)(1 - 2\rho) \frac{d\rho}{dx} \\ + \Omega_a(1 - \rho)(1 - \rho_d) + \Omega_{ad}(1 - \rho)\rho_d - \Omega_d\rho = 0. \end{aligned} \quad (11)$$

B. Numerical scheme

Since our system is complex due to the presence of dynamic disorder along with particle nonconserving dynamics, it is difficult to obtain the analytical solution of differential equation (11). Numerical techniques have been widely used in the literature in order to get approximate solutions of such complex systems [31,39]. The time derivative term is kept in the system and the steady-state solution is captured at very large values of n . The model equation is discretized by using a finite difference scheme, applying the first-order forward difference formula for the time derivative and the center difference of first and second order for space derivatives, which gives

$$\begin{aligned} \rho_i^{n+1} &= \rho_i^n + \frac{\epsilon}{2} \frac{\Delta t'}{\Delta x^2} (p - p\rho_{i,d}^n + p_d\rho_{i,d}^n) (\rho_{i+1}^n - 2\rho_i^n + \rho_{i-1}^n) \\ &\quad + \frac{\Delta t'}{2\Delta x} (-p + 2p\rho_i + p\rho_{i,d}^n - 2p\rho_i\rho_{i,d}^n - p_d\rho_{i,d}^n \\ &\quad + 2p_d\rho_i\rho_{i,d}^n) (\rho_{i+1}^n - \rho_{i-1}^n) \\ &\quad + \Delta t' [\Omega_a(1 - \rho_i^n)(1 - \rho_{i,d}^n) + \Omega_{ad}(1 - \rho_i^n)\rho_{i,d}^n \\ &\quad - \Omega_d\rho_i^n]. \end{aligned} \quad (12)$$

C. Monte Carlo simulations

To test the validity of the results given by the continuum mean-field approximation, Monte Carlo simulations are performed. Random sequential update rules are used, taking lattice length $L = 1000$. The Monte Carlo simulations are carried out for 10^9 time steps and also the first 5% of time steps are ignored to ensure the occurrence of steady state. The stationary state density has been obtained with a typical time interval of $10L$ between each step of average. The upcoming section shows the comparison of our theoretical findings using the mean-field approximation with those of Monte Carlo simulations.

V. RESULTS AND DISCUSSION

In this section, we explore the steady-state behavior of dynamically disordered TASEP with LK. The dynamics of the system are mostly governed by the following parameters: the defect binding rate k_+ , the defect unbinding rate k_- , attachment rates Ω_a, Ω_{ad} , and detachment rate Ω_d . To investigate the role of each of these parameters in a comprehensive way, the results have been represented in the form of phase diagrams and density profiles obtained using a numerical scheme for the continuum mean-field equations,

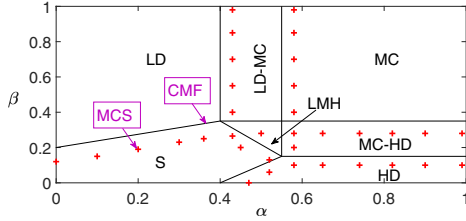


FIG. 2. Steady-state phase diagram with seven different phases for $k_+ = 0.4$, $k_- = 0.8$, $p_d = 1/3$, $K = 1$, $\Omega = 0.2$, and $\Omega_{ad} = \Omega/2$. The markers are results from Monte Carlo simulations (MCS) and the solid lines are results from continuum mean-field (CMF) approximation. The LMH region corresponds to LD-MC-HD.

and are further validated with Monte Carlo simulations. For the numerical solution, the values of $\Delta t' = 0.0005$, $\Delta x = 1/L = 0.001$ have been chosen, which satisfy the stability condition $|\frac{\Delta t'}{\Delta x}| \leq 1$ [40].

We found in the literature that, for exclusion processes with particle nonconserving dynamics (LK), the stationary state dynamics of the system is characterized in terms of the binding constant K defined as $K = \omega_a/\omega_d$ [15]. In this study, our focus is on analyzing the dynamics of the system for two different values, $K = 1$ and $K = 3$.

A. $K = 1$

For simplicity, first we explored the symmetric case in which the attachment and detachment rates of particles are taken as equal, i.e., $\Omega_a = \Omega_d = \Omega$. Without loss of generality, the attachment rate in the presence of a defect at the target site (Ω_{ad}) is taken as half the attachment rate in the absence of a defect at the target site (Ω_a), i.e., $\Omega_{ad} = \Omega_a/2$ throughout the paper.

The phase diagram for $\Omega = 0.2$, $k_+ = 0.4$, and $k_- = 0.8$ has been sketched in Fig. 2, where the solid lines represent transitions between different phases obtained using numerical solution of the continuum mean-field equations, and corresponding markers represent phase transitions using Monte Carlo simulations. The deviations in results of Monte Carlo simulations and the finite difference scheme are due to approximations used in mean field approach which ignore the interactions in neighboring sites. The corresponding density and current profiles are shown in Figs. 3 and 4 respectively. Evidently, the following inferences can be drawn from the phase diagram.

(i) It can be seen that there exist seven different phases in the steady state of the system which are the combinations of low density phase (LD), maximal current phase (MC), and high density phase (HD) where LD characterizes average density less than $1/2$, HD characterizes average density greater than $1/2$, and MC has average density equal to $1/2$ [10].

(ii) Another characteristic of phase diagram is an appearance of shock phase in a ddTASEP with LK which otherwise is not noticed in single-channel and two-channel ddTASEP without LK [38,39].

(iii) Unlike the existence of three phases [LD, MC, and HD in Figs. 3(a), 3(c) and 3(d) respectively] in ddTASEP without LK [38], the nonequilibrium phenomenon of phase coexistence has been observed. The bulk transitions in the

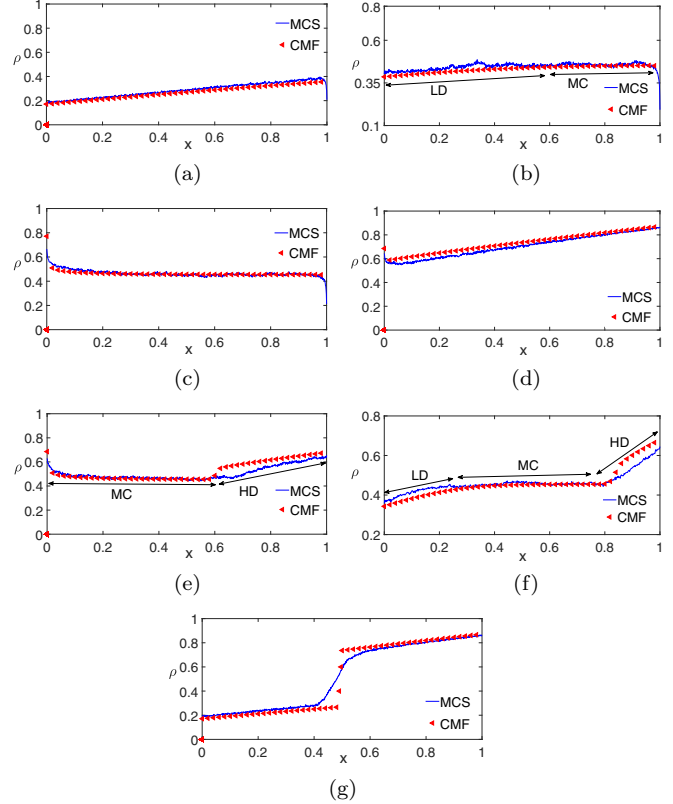


FIG. 3. Density profiles for $p_d = 1/3$, $k_+ = 0.4$, $k_- = 0.8$, $\Omega = 0.2$, $\Omega_{ad} = \Omega/2$. and $L = 1000$. (a) LD phase for $\alpha = 0.2$, $\beta = 0.8$, (b) LD-MC phase for $\alpha = 0.45$, $\beta = 0.9$, (c) MC phase for $\alpha = 0.9$, $\beta = 0.85$, (d) HD phase for $\alpha = 0.8$, $\beta = 0.1$, (e) MC-HD phase for $\alpha = 0.8$, $\beta = 0.25$, (f) LD-MC-HD phase for $\alpha = 0.4$, $\beta = 0.25$, and (g) S phase for $\alpha = 0.2$, $\beta = 0.1$. The solid lines (blue) indicate the density profiles obtained through Monte Carlo simulations (MCS) and triangles (red) are profiles from continuum mean-field (CMF) approximation.

phase plane lead to the existence of a three-phase coexistence region (LD-MC-HD) in Fig. 3(f) and the two-phase coexistence regions namely (S, LD-MC, and MC-HD) Figs. 3(g), 3(b), and 3(e) respectively. All the transitions between different phases in the diagrams are continuous.

(iv) On comparing the results with homogeneous single-channel TASEP with LK [15], the phase diagrams are found to be qualitatively similar. However, there are a few differences in the density and current profiles due to the dynamic disorder clearly shown in Figs. 3 and 4 respectively.

In general the bulk particle density $\rho = 1/2$ and the current $J = 1/4$ in the MC phase in homogeneous TASEP [10]. Interestingly, in the current model, the bulk particle density in the MC phase remains slightly less than $1/2$. This decrease might be due to the presence of dynamic defects in the system.

Figure 4 represents current profiles corresponding to different density profiles shown in Fig. 3. The current in pure LD, MC, and HD phases for given sets of parameters can be seen in Figs. 4(a), 4(c), and 4(d) respectively. Although the magnitude of particle current in the MC phase is less than $1/4$, we continue to name this the MC phase as per convention used in the literature [13,31,38,39]. Figures 4(b) and 4(e)

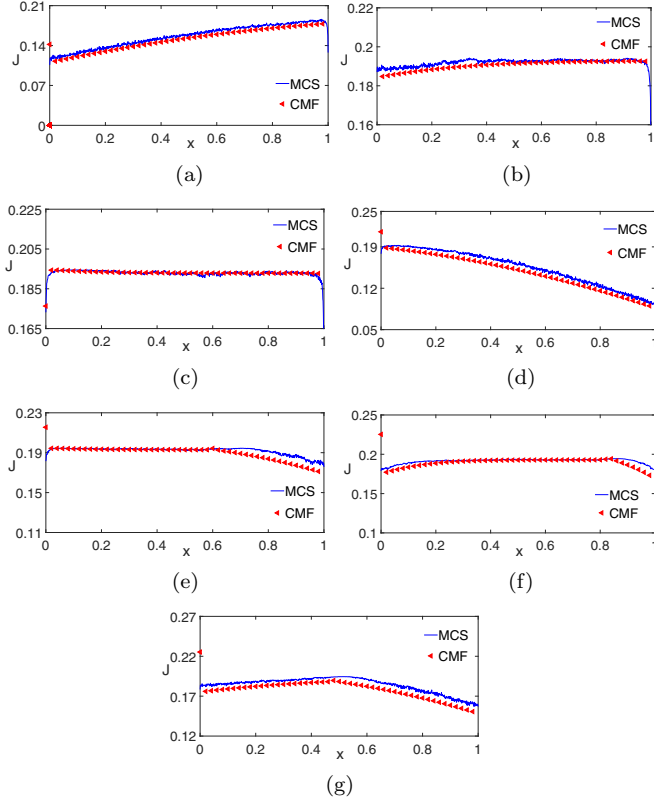


FIG. 4. Current profiles for $p_d = 1/3$, $k_+ = 0.4$, $k_- = 0.8$, $\Omega = 0.2$, $\Omega_{ad} = \Omega/2$, and $L = 1000$. (a) LD phase for $\alpha = 0.2$, $\beta = 0.8$, (b) LD-MC phase for $\alpha = 0.45$, $\beta = 0.9$, (c) MC phase for $\alpha = 0.9$, $\beta = 0.85$, (d) HD phase for $\alpha = 0.8$, $\beta = 0.1$, (e) MC-HD phase for $\alpha = 0.8$, $\beta = 0.25$, (f) LD-MC-HD phase for $\alpha = 0.4$, $\beta = 0.25$, and (g) S phase for $\alpha = 0.2$, $\beta = 0.1$. The solid lines (blue) indicate the current profiles obtained through Monte Carlo simulations (MCS) and triangles (red) are profiles from continuum mean-field (CMF) approximation.

show current for two-phase coexistence regions LD-MC and MC-HD respectively. In the LD-MC phase the current first increases and then at the transition point of LD to MC it reaches its maximum value. A similar observation is made for the HD-MC phase. The current corresponding to density in LD-MC-HD and S phases is shown in Figs. 4(f) and 4(g) respectively. The current profile has a transition point located at the position of shock in the plane.

1. Elimination of phases

Figure 5 represents the phase diagram for different values of Ω with all other parameter values the same. Figures 5(a) and 5(b) correspond to $\Omega = 0.5$ and $\Omega = 1$ respectively. It has been found that the number of phases decreases in the phase plane on increasing Ω . The LD and HD phases disappear, leaving behind only five phases. The process of elimination of pure LD and HD phases with an increase in Ω is found to be similar to single-channel TASEP with LK [15], which is due to localization of shock in the bulk. A similar trend continues on increasing Ω to 1, in which the phase diagram comprises only four phases.

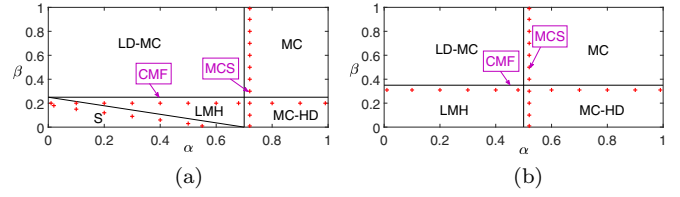


FIG. 5. Phase diagram for $k_+ = 0.4$, $k_- = 0.8$, $p_d = 1/3$, $K = 1$, $\Omega_{ad} = \Omega/2$; (a) $\Omega = 0.5$ and (b) $\Omega = 1$. The markers are results from Monte Carlo simulations (MCS) and the solid lines are results from continuum mean-field (CMF) approximation. The LMH region corresponds to LD-MC-HD.

2. Effect of defect binding and unbinding rates

Another set of important parameters controlling the steady-state behavior are the defect binding and unbinding rates (k_+ and k_-). Their values control the defect density $\rho_d = k_+/(k_+ + k_-)$ in the system which further affects not only the particle density ρ but also the current J . For $k_+ = 0.4$ and $k_- = 0.8$, $\rho_d = 1/3$.

Figure 6(a) represents the phase diagram for $\Omega = 0.2$, $k_+ = 0.15$, and $k_- = 0.1$. On comparing Figs. 2 and 6(a), the significant effect is shifting of phase boundaries in the phase plane which leads to elimination of the HD phase. Note that here the value of defect density $\rho_d = 0.6$.

Upon increasing the defect density ρ_d to 0.9 by choosing $k_+ = 0.9$ and $k_- = 0.1$, a significantly different phase diagram is obtained, as shown in Fig. 6(b). The phase diagram only consists of two phases, namely LD and S. With the increase in the defect density in the system, there is a relative decrease in the particle density because of which the LD phase is expanded over a larger area in the phase plane. The effect of varying k_+ and k_- is found to be similar for $\Omega = 0.5$ and $\Omega = 1$.

3. Variation in strength of dynamic defect

In the previous subsection, we have examined the effect of defect binding and unbinding rates (k_+ , k_-) which control the defect density in the system. Another parameter related to defect dynamics is the slow hopping rate of particle p_d , which indicates the strength of defect. Lowering the value of p_d , the defect becomes stronger. Further, the strength of defect regulates the particle density in the system.

Figure 7 shows the density profiles for $\alpha = 0.42$, $\beta = 0.9$, $k_+ = 0.4$, and $k_- = 0.8$ with three different values of p_d .

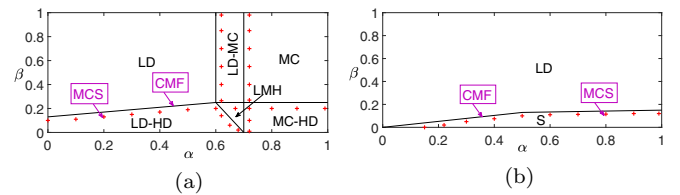


FIG. 6. Phase diagram for $p_d = 1/3$, $K = 1$, $\Omega = 0.2$, $\Omega_{ad} = \Omega/2$; (a) $k_+ = 0.15$, $k_- = 0.1$ and (b) $k_+ = 0.9$, $k_- = 0.1$. The markers are results from Monte Carlo simulations (MCS) and the solid lines are results from continuum mean-field (CMF) approximation. The LMH region corresponds to LD-MC-HD.

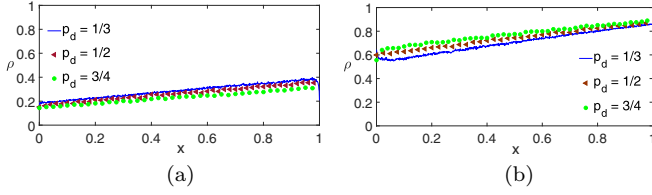


FIG. 7. Density profile for $K = 1, k_+ = 0.4, k_- = 0.8$, and varying p_d ; (a) $\alpha = 0.2, \beta = 0.8$ and (b) $\alpha = 0.8, \beta = 0.1$.

There is only a minor quantitative effect observed by varying the defect strength in the system. A decrease in the magnitude of particle density ρ in the LD phase [Fig. 7(a)] and an increase in the magnitude of particle density in the HD phase [Fig. 7(b)] have been found by increasing the defect strength. Apart from these changes, there are no noticeable changes in the phase diagrams except for minor shifting in the phase boundaries.

B. $K = 3$

This section explains the steady-state dynamics for $K = 3$. The phase diagram for $\Omega_a = 0.2, k_+ = 0.4$, and $k_- = 0.8$ is shown in Fig. 8. On comparing the phase diagram for $K = 1$ and $K = 3$ (Figs. 2 and 8) with all other parameter values the same, the following observations can be listed.

(i) Clearly, the number of phases decreases in the steady state of the system upon increasing K . Only four phases are found for $K = 3$, which are LD, S, HD, and MC phases. The coexisting phases completely disappear. This phenomenon of reduction of phases is similar to the one observed for homogeneous single-channel TASEP with LK [15].

(ii) Interestingly, the phase diagram is qualitatively similar to the one in homogeneous single-channel TASEP with LK [15].

(iii) Similar to the MC phase for $K = 1$, here also the current in the MC phase is less than $1/4$.

Figure 9 shows the density profiles corresponding to four different regions in the phase diagram. Here also it is found that with an increase in the magnitude of particle density there is a decrease in maximal current in the system.

1. Disappearance of LD phase

To examine the effect of Ω_a , the phase diagrams for different values of Ω_a have been plotted in Fig. 10. Upon an

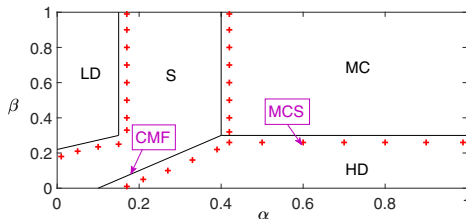


FIG. 8. Steady-state phase diagram with four different phases for $k_+ = 0.4, k_- = 0.8, p_d = 1/3, K = 3, \Omega_a = 0.2$, and $\Omega_{ad} = \Omega/2$. The markers are results from Monte Carlo simulations (MCS) and the solid lines are results from continuum mean-field (CMF) approximation.

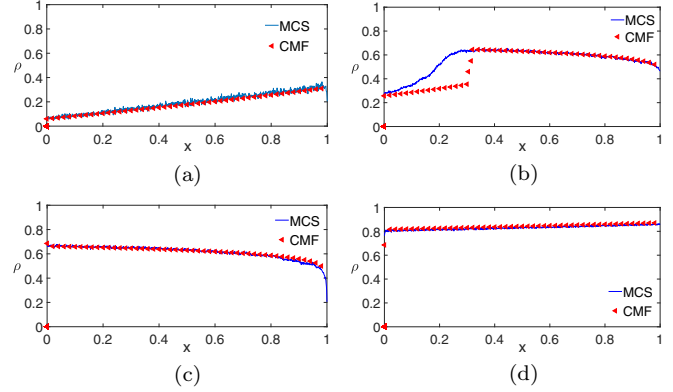


FIG. 9. Density profiles for $p_d = 1/3, k_+ = 0.4, k_- = 0.8, K = 3, \Omega_a = 0.2, \Omega_{ad} = \Omega/2$ and $L = 1000$; (a) LD phase for $\alpha = 0.07, \beta = 0.8$, (b) S phase for $\alpha = 0.3, \beta = 0.4$, (c) MC phase for $\alpha = 0.8, \beta = 0.9$, (d) HD phase for $\alpha = 0.8, \beta = 0.1$. The solid lines (blue) indicate the density profiles obtained through Monte Carlo simulations (MCS) and triangles (red) are profiles from continuum mean-field (CMF) approximation.

increase in Ω_a , one can observe the reduction in number of phases in the phase plane due to elimination of the LD phase. This is because an increase in the number of particles getting attached to the lattice hinders the forward motion of particles and consequently particles stay for longer time on the lattice causing high density. On further increase in the value of $\Omega_a = 1$ the phase diagram remains almost the same as that for $\Omega = 0.5$.

2. Effect of defect binding and unbinding rates

To examine the effect of defect binding and unbinding rates, the phase diagrams have been plotted for different values of k_+, k_- at $\Omega_a = 0.2$. Figure 11(a) represents the phase diagram for $\Omega = 0.2$ and for $k_+ = 0.15, k_- = 0.1$. On comparing Figs. 8 and 11(a), the significant observation is shifting of phase boundaries in the phase plane whereas qualitatively the phase diagrams remain the same. Also, the number of phases remains identical. This effect is equivalent to that observed for the same parameters under $K = 1$. Additionally, this effect is similar to the analogous model of dynamically disordered TASEP without nonconserving dynamics [15].

The phase diagram observed for $\rho_d = 0.9$ taking $k_+ = 0.9$ and $k_- = 0.1$ is shown in Fig. 11(b). The S phase is observed to be expanded over a larger area in the phase plane which might be due to increase in the defect density in the system

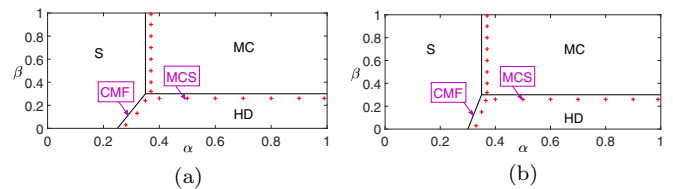


FIG. 10. Phase diagram for $k_+ = 0.4, k_- = 0.8, p_d = 1/3, K = 3, \Omega_{ad} = \Omega/2$, (a) $\Omega_a = 0.5$, and (b) $\Omega_a = 1$. The markers are results from Monte Carlo simulations (MCS) and the solid lines are results from continuum mean-field (CMF) approximation.

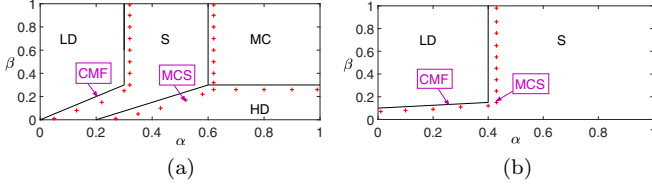


FIG. 11. Phase diagram for $p_d = 1/3$, $K = 3$, $\Omega_a = 0.2$, $\Omega_{ad} = \Omega_a/2$; (a) $k_+ = 0.15$, $k_- = 0.1$ and (b) $k_+ = 0.9$, $k_- = 0.1$. The markers are results from Monte Carlo simulations (MCS) and the solid lines are results from continuum mean-field (CMF) approximation.

and larger value of binding constant K . Also the trend continues for $\Omega = 0.5$ and $\Omega = 1$.

Apart from this, it is observed that on varying slow hopping rate p_d there is a qualitative minor change in the density profiles which is similar to that for $K = 1$.

VI. SHOCK DYNAMICS

We explore the effect of defect density on shock and the results are shown in Fig. 12. It is clearly found that the shock moves from left to right boundaries upon increasing defect density on the lattice. This is because the particle density decreases with increasing density of defects in the system. Consequently, the HD phase is found to be eliminated whereas the LD phase expands. This observation can be validated from the phase diagrams (Figs. 2 and 6). The trend has been found to be similar using Monte Carlo simulations and continuum mean-field approximation.

Further, shock profile has been examined by varying the defect strength (p_d). Figure 13 shows the density profile for $\alpha = 0.3$, $\beta = 0.4$, $k_+ = 0.4$, and $k_- = 0.8$ with three different values of p_d . A change in the shock position has been noticed upon varying p_d . Lowering the value of p_d , the defect becomes stronger and the blockage of particles increases, leading to an increase in the HD profile on the lattice. Hence the shock continuously changes its position from right to left boundaries of the system. Further, Monte Carlo simulations and continuum mean-field approximation give similar observations.

Effect of system size

The effect of system size on the steady state density profiles has been analyzed. Extensive Monte Carlo simulations have

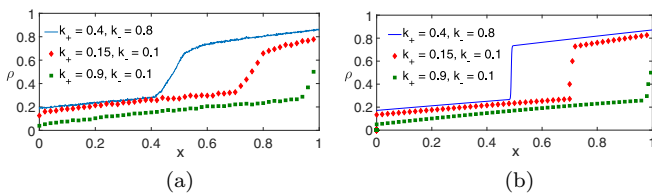


FIG. 12. Shock profile for $K = 1$, $\Omega_a = 0.2$, $p_d = 1/3$, $\alpha = 0.2$, $\beta = 0.1$, and varying k_+ and k_- . The results are captured using (a) Monte Carlo simulations and (b) continuum mean-field approximation.

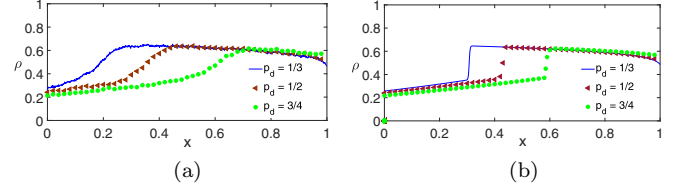


FIG. 13. Shock profile for $K = 3$, $\Omega_a = 0.2$, $k_+ = 0.4$, $k_- = 0.8$, $\alpha = 0.3$, $\beta = 0.4$, and varying p_d . The results are captured using (a) Monte Carlo simulations and (b) continuum mean-field approximation.

been carried out taking $L = 500$, 1000 , 5000 , and 10000 for different set of system parameters which are found to have no significant effect on the density profiles. Figures 14(a) and 14(b) show the results for shock profiles from Monte Carlo simulations and the continuum mean-field approximation respectively. It is clearly found that the results are not affected by system size.

VII. CONCLUSION

In this paper, we have attempted to study the role played by Langmuir kinetics in a single-channel dynamically disordered exclusion process. The unconstrained system with open boundary conditions is considered, in which a defect can bind to a site irrespective of presence or absence of a particle at that site. The motivation behind this model is the biological process of gene transcription in which the DNA binding proteins and the low concentration of tRNA act as disorder. This hindrance slows the transport of cargoes, causing jamming of molecular motors on DNA track. The continuum mean-field equations are employed to obtain steady-state phase diagrams and density profiles. The finite difference scheme is used to solve the mean-field equations, which otherwise are difficult to solve analytically due to the presence of dynamic disorder and LK. A random sequential update rule is used to carry out Monte Carlo simulations of the system. The computational results are in good agreement with numerical results.

The competing interplay between dynamic disorder and LK results in rich steady-state phase diagrams consisting of pure and coexisting phases. Another considerable outcome due to the presence of LK dynamics is the appearance of steady-state shock which otherwise is not found in the single-channel ddTASEP without LK. The system is explored for two values of binding constant, $K = 1$ and $K = 3$. The effect of binding constant Ω_a is examined on the phase diagrams and it

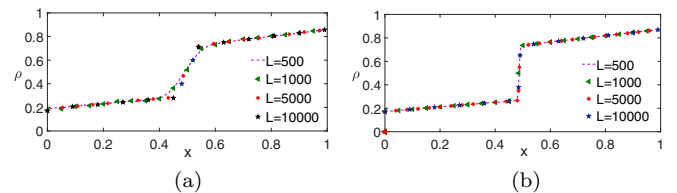


FIG. 14. Effect of system size for $\alpha = 0.2$, $\beta = 0.1$, $k_+ = 0.4$, $k_- = 0.8$, $K = 1$, $\Omega = 0.2$, $\Omega_{ad} = \Omega/2$, and $L = 500$, 1000 , 5000 , and 10000 . The results are obtained using (a) Monte Carlo simulations and (b) continuum mean field approximations.

is found that an increasing Ω_a reduces the number of phases in the system, which is due to localization of shock in the bulk. Further, the defect binding and unbinding rates are observed to shift phase boundaries in the plane, with the number of phases remaining identical. For large value of defect density in the system the phase diagram consists of only two phases, namely LD and S, which is due to low particle density on the lattice. Moreover, effect of variation in defect strength is observed on density profiles. It has been observed that with an increase in defect strength, the particle density in the LD phase decreases whereas in the HD phase the particle density increases. These mentioned findings are similar for both values

of binding constant K . The shock dynamics are explored by varying defect density and the defect strength in the system. The shock moves from right to left upon increasing defect strength on the lattice. Also, the steady-state results are found to be independent of system size.

Here, we focused on a complete study of steady-state properties of a single-channel dynamically disordered TASEP system with LK under unconstrained conditions. In the future, the single-channel model can be generalized to a two-channel model that might uncover other interesting features of the steady-state behavior of the system.

-
- [1] A. B. Kolomeisky, *Motor Proteins and Molecular Motors* (CRC, Boca Raton, FL, 2015).
- [2] N. G. Van Kampen, *Stochastic Processes in Physics and Chemistry* (Elsevier, Amsterdam, 1992), Vol. 1.
- [3] T. Chou and G. Lakatos, Clustered Bottlenecks in mRNA Translation and Protein Synthesis, *Phys. Rev. Lett.* **93**, 198101 (2004).
- [4] M. A. Sørensen, C. Kurland, and S. Pedersen, Codon usage determines translation rate in escherichia coli, *J. Mol. Biol.* **207**, 365 (1989).
- [5] C. M. Stenström, H. Jin, L. L. Major, W. P. Tate, and L. A. Isaksson, Codon bias at the 3'-side of the initiation codon is correlated with translation initiation efficiency in escherichia coli, *Gene* **263**, 273 (2001).
- [6] C. T. MacDonald and J. H. Gibbs, Concerning the kinetics of polypeptide synthesis on polyribosomes, *Biopolymers: Original Res. Biomol.* **7**, 707 (1969).
- [7] C. T. MacDonald, J. H. Gibbs, and A. C. Pipkin, Kinetics of biopolymerization on nucleic acid templates, *Biopolymers: Original Res. Biomol.* **6**, 1 (1968).
- [8] M. Schliwa and G. Woehlke, Molecular motors: Switching on kinesin, *Nature (London)* **411**, 424 (2001).
- [9] T. Chou, K. Mallick, and R. Zia, Non-equilibrium statistical mechanics: From a paradigmatic model to biological transport, *Rep. Prog. Phys.* **74**, 116601 (2011).
- [10] A. Schadschneider, D. Chowdhury, and K. Nishinari, *Stochastic Transport in Complex Systems: From Molecules to Vehicles* (Elsevier, Amsterdam, 2010).
- [11] J. Krug, Boundary-Induced Phase Transitions in Driven Diffusive Systems, *Phys. Rev. Lett.* **67**, 1882 (1991).
- [12] G. Schütz and E. Domany, Phase transitions in an exactly soluble one-dimensional exclusion process, *J. Stat. Phys.* **72**, 277 (1993).
- [13] A. B. Kolomeisky, G. M. Schütz, E. B. Kolomeisky, and J. P. Straley, Phase diagram of one-dimensional driven lattice gases with open boundaries, *J. Phys. A: Math. Gen.* **31**, 6911 (1998).
- [14] A. Parmeggiani, T. Franosch, and E. Frey, Phase Coexistence in Driven One-Dimensional Transport, *Phys. Rev. Lett.* **90**, 086601 (2003).
- [15] A. Parmeggiani, T. Franosch, and E. Frey, Totally asymmetric simple exclusion process with Langmuir kinetics, *Phys. Rev. E* **70**, 046101 (2004).
- [16] N. Mirin and A. B. Kolomeisky, Effect of detachments in asymmetric simple exclusion processes, *J. Stat. Phys.* **110**, 811 (2003).
- [17] V. Popkov, A. Rákos, R. D. Willmann, A. B. Kolomeisky, and G. M. Schütz, Localization of shocks in driven diffusive systems without particle number conservation, *Phys. Rev. E* **67**, 066117 (2003).
- [18] S. Mukherji and S. M. Bhattacharjee, Nonequilibrium criticality at shock formation in steady states, *J. Phys. A: Math. Gen.* **38**, L285 (2005).
- [19] R. Jiang, R. Wang, and Q.-S. Wu, Two-lane totally asymmetric exclusion processes with particle creation and annihilation, *Physica A* **375**, 247 (2007).
- [20] R. Wang, R. Jiang, M. Liu, J. Liu, and Q.-S. Wu, Effects of Langmuir kinetics on two-lane totally asymmetric exclusion processes of molecular motor traffic, *Int. J. Mod. Phys. C* **18**, 1483 (2007).
- [21] A. K. Gupta and I. Dhiman, Asymmetric coupling in two-lane simple exclusion processes with Langmuir kinetics: Phase diagrams and boundary layers, *Phys. Rev. E* **89**, 022131 (2014).
- [22] I. Dhiman and A. K. Gupta, Effect of coupling strength on a two-lane partially asymmetric coupled totally asymmetric simple exclusion process with Langmuir kinetics, *Phys. Rev. E* **90**, 012114 (2014).
- [23] A. B. Kolomeisky, Asymmetric simple exclusion model with local inhomogeneity, *J. Phys. A: Math. Gen.* **31**, 1153 (1998).
- [24] L. B. Shaw, R. K. P. Zia, and K. H. Lee, Totally asymmetric exclusion process with extended objects: A model for protein synthesis, *Phys. Rev. E* **68**, 021910 (2003).
- [25] S. A. Janowsky and J. L. Lebowitz, Finite-size effects and shock fluctuations in the asymmetric simple-exclusion process, *Phys. Rev. A* **45**, 618 (1992).
- [26] P. Greulich and A. Schadschneider, Phase diagram and edge effects in the ASEP with bottlenecks, *Physica A* **387**, 1972 (2008).
- [27] J. Dong, B. Schmittmann, and R. Zia, Towards a model for protein production rates, *J. Stat. Phys.* **128**, 21 (2007).
- [28] G. Tripathy and M. Barma, Steady State and Dynamics of Driven Diffusive Systems with Quenched Disorder, *Phys. Rev. Lett.* **78**, 3039 (1997).
- [29] M. E. Foulaadvand, A. B. Kolomeisky, and H. Teymouri, Asymmetric exclusion processes with disorder: Effect of correlations, *Phys. Rev. E* **78**, 061116 (2008).

- [30] K. Qiu, X. Yang, W. Zhang, D. Sun, and Y. Zhao, Density profiles in the totally asymmetric exclusion processes with both local inhomogeneity and Langmuir kinetics, *Physica A* **373**, 1 (2007).
- [31] I. Dhiman and A. K. Gupta, Collective dynamics of an inhomogeneous two-channel exclusion process: Theory and Monte Carlo simulations, *J. Comput. Phys.* **309**, 227 (2016).
- [32] H. Soh and M. Ha, Passive tracer dynamics in slow-bond problem, *J. Stat. Mech.: Theory Exp.* (2019) 094009.
- [33] H. Soh, M. Ha, and H. Jeong, Jamming and condensation in one-dimensional driven flow, *Phys. Rev. E* **97**, 032120 (2018).
- [34] H. Soh, Y. Baek, M. Ha, and H. Jeong, Effects of a local defect on one-dimensional nonlinear surface growth, *Phys. Rev. E* **95**, 042123 (2017).
- [35] M. Ha, J. Timonen, and M. den Nijs, Queuing transitions in the asymmetric simple exclusion process, *Phys. Rev. E* **68**, 056122 (2003).
- [36] N. Hao, S. Krishna, A. Ahlgren-Berg, E. E. Cutts, K. E. Shearwin, and I. B. Dodd, Road rules for traffic on DNA-systematic analysis of transcriptional roadblocking in vivo, *Nucleic Acids Res.* **42**, 8861 (2014).
- [37] V. Epshtein, F. Toulmé, A. R. Rahmouni, S. Borukhov, and E. Nudler, Transcription through the roadblocks: The role of RNA polymerase cooperation, *EMBO J.* **22**, 4719 (2003).
- [38] B. Waclaw, J. Cholewa-Waclaw, and P. Greulich, Totally asymmetric exclusion process with site-wise dynamic disorder, *J. Phys. A: Math. Theor.* **52**, 065002 (2019).
- [39] S. Garg and I. Dhiman, Two-channel totally asymmetric simple exclusion process with site-wise dynamic disorder, *Physica A* **545**, 123356 (2020).
- [40] G. D. Smith, G. D. Smith, and G. D. S. Smith, *Numerical Solution of Partial Differential Equations: Finite Difference Methods* (Oxford University Press, Oxford, 1985).